

Theoretical study on the radical–radical reaction mechanism of $\text{CH}_2\text{I} + \text{NO}_2$

Xiu-Juan Jia · You-Jun Liu · Jing-Yu Sun ·
Hao Sun · Fang Wang · Xiu-Mei Pan ·
Rong-Shun Wang

Received: 16 September 2009 / Accepted: 17 November 2009 / Published online: 3 December 2009
© Springer-Verlag 2009

Abstract The mechanisms of CH_2I with NO_2 reaction were investigated on the singlet and triplet potential energy surfaces (PESs) by the UB3LYP method. The energetic information is further refined at the UCCSD(T) and UQCISD(T) levels of theory. Our results indicated that the title reaction is more favorable on the singlet PES thermodynamically, and less competitive on the triplet one. On the singlet PES, the title reaction is most likely to be initiated by the carbon-to-oxygen approach forming the adduct IM1 ($\text{H}_2\text{ICONO-}trans$) without any transition state, which can isomerizes to IM2 (H_2ICNO_2) and IM3 ($\text{H}_2\text{ICONO-}cis$), respectively. The most feasible pathway is the 1, 3-I shift with C–I and O–N bonds cleavage along with the N–I bond formation of IM1 lead to the product P1 ($\text{CH}_2\text{O} + \text{INO}$), which can further dissociate to give P3 ($\text{CH}_2\text{O} + \text{I} + \text{NO}$). The competitive pathway is 1, 3-H shift associated with O–N bond rupture of IM1 to form P2 ($\text{CHIO} + \text{HNO}$). The theoretically obtained major product CH_2O and adducts IM1 and IM2 are in good agreement with the kinetic detection in experiment. The similarities

and discrepancies between $\text{CH}_2\text{I} + \text{NO}_2$ and $\text{CH}_2\text{Br} + \text{NO}_2$ reactions are discussed in terms of the electronegativity of halogen atom and the barrier height of the rate-determining process. The present study may be helpful for further experimental investigation of the title reaction.

Keywords Reaction mechanism · Potential energy surface (PES) · $\text{CH}_2\text{I} \cdot \text{NO}_2$

1 Introduction

Iodomethane is known to be an important source of the reactive I atom, which may further react with O_3 to produce IO radicals under atmospheric conditions [1]. IO_x (I and IO) cycles have been demonstrated to participate in ozone destruction in the marine boundary layer and also in the troposphere [2]. The natural source of iodomethane has been identified as pelagic ocean [3] and a marine phytoplankton [4]. CH_2I radical is a key species in the atmospheric chemistry of iodinated compounds, since it is generated by photolysis and chemical reactions involving the most abundant CH_3I and CH_2I_2 , such as reaction with OH or Cl. Nitrogen oxides, known to be the major atmospheric pollutants released by combustion process, have attracted extensive attentions both experimentally and theoretically. In order to minimize the harmful effects before their release in the atmosphere, one effective way is to reduce them chemically by their reactions with other species [5–8]. Reactions with NO_2 can be expected to be important during the oxidation of halogenated compounds at low temperature, because traces of nitrogen oxides are also often present [9].

Reliable information on the kinetics of these halogenated methyl radical reactions is of importance for the

X.-J. Jia · J.-Y. Sun · H. Sun · F. Wang · X.-M. Pan (✉) ·
R.-S. Wang (✉)

Faculty of Chemistry, Institute of Functional Material Chemistry, Northeast Normal University,
130024 Changchun, People's Republic of China
e-mail: panxm460@nenu.edu.cn

R.-S. Wang
e-mail: wangrs@nenu.edu.cn

X.-J. Jia
e-mail: jiaxj753@nenu.edu.cn

Y.-J. Liu
Faculty of Physics, Aviation University of Air Force,
130022 Changchun, People's Republic of China

modeling of NO_x -involved reaction processes. Recently, Timonen et al. [10] reported for the first time the rate constants of $\text{CH}_2\text{I} + \text{NO}_2$ reactions over the temperature ranges (221–363 K) using a laser photolysis/photoionization mass spectrometry and derived the rate constant expression as $(2.18 \pm 0.07) \times 10^{-11} (T/300 \text{ K})^{-1.45 \pm 0.22} \text{ cm}^3 \text{ mol}^{-1} \text{ s}^{-1}$. The CH_2O was the observed product. In addition, a relatively weak signal for the formation of iodonitromethane (CH_2INO_2) or iodomethyl nitrite (CH_2IONO) product was observed as well as NO. But the available information on product channels, product distributions, and reaction mechanism was not further provided though this information may be important in the NO_2 -involved sequential chain processes. In addition, very recently, we have built up the potential energy surface (PES) of the analogous $\text{CH}_2\text{Br} + \text{NO}_2$ reaction [11]. Then, the question arise: is the mechanism of the title reaction similar to that of the $\text{CH}_2\text{Br} + \text{NO}_2$ reaction or not?

To our best knowledge, no theoretical study has been reported for the title reaction. Therefore, it is highly desirable to carry out the detailed theoretical study on the PES of the title reaction in view of the potential importance and the rather limited information. The aim of the present study was to (1) provide the elaborate isomerization and dissociation channels on the CH_2IONO PES; (2) investigate the products of the title reaction to assist in further experimental identification; (3) make comparisons between the reactions of CH_2X ($\text{X} = \text{Br}$ and I) to deeply understand the halogenated methyl chemistry.

2 Computational methods

All calculations are carried out using the GAUSSIAN 03 program packages [12]. The geometries of all the reactants, products, intermediates, and transition states are optimized using the hybrid density functional UB3LYP method (Becke's three parameter hybrid functional with the non-local correlation functional of Lee et al.) [13, 14] in conjunction with the 6-31+G(d, p) basis set for the elements H, C, O, and N. For iodine, the triple- ζ member of systematically convergent basis sets containing a small core pseudopotential (aug-cc-pVTZ-PP) was employed [15, 16]. These basis sets are referred to as basis set I. Frequency calculations were performed on all optimized structures. These frequency calculations verify that all minima are real and that all transition states have one imaginary frequency. The zero-point energy (ZPE) corrections are obtained at the same level of theory.

In order to obtain more reliable energetic data, higher level single-point energy calculations are performed using UCCSD(T) and UQCISD(T) method with larger basis set [6-311G(d, p)] for the elements H, C, O, and N and with

aug-cc-pVTZ-PP for iodine using the UB3LYP/I optimized geometries. These basis sets are referred to as basis set II. To confirm that the transition states connect designated intermediates, intrinsic reaction coordinate (IRC) calculation [17, 18] is carried out at the UB3LYP/I level of theory. Moreover, unless otherwise specified, the UCCSD(T)/II single-point energies with ZPE corrections are used in the following discussions.

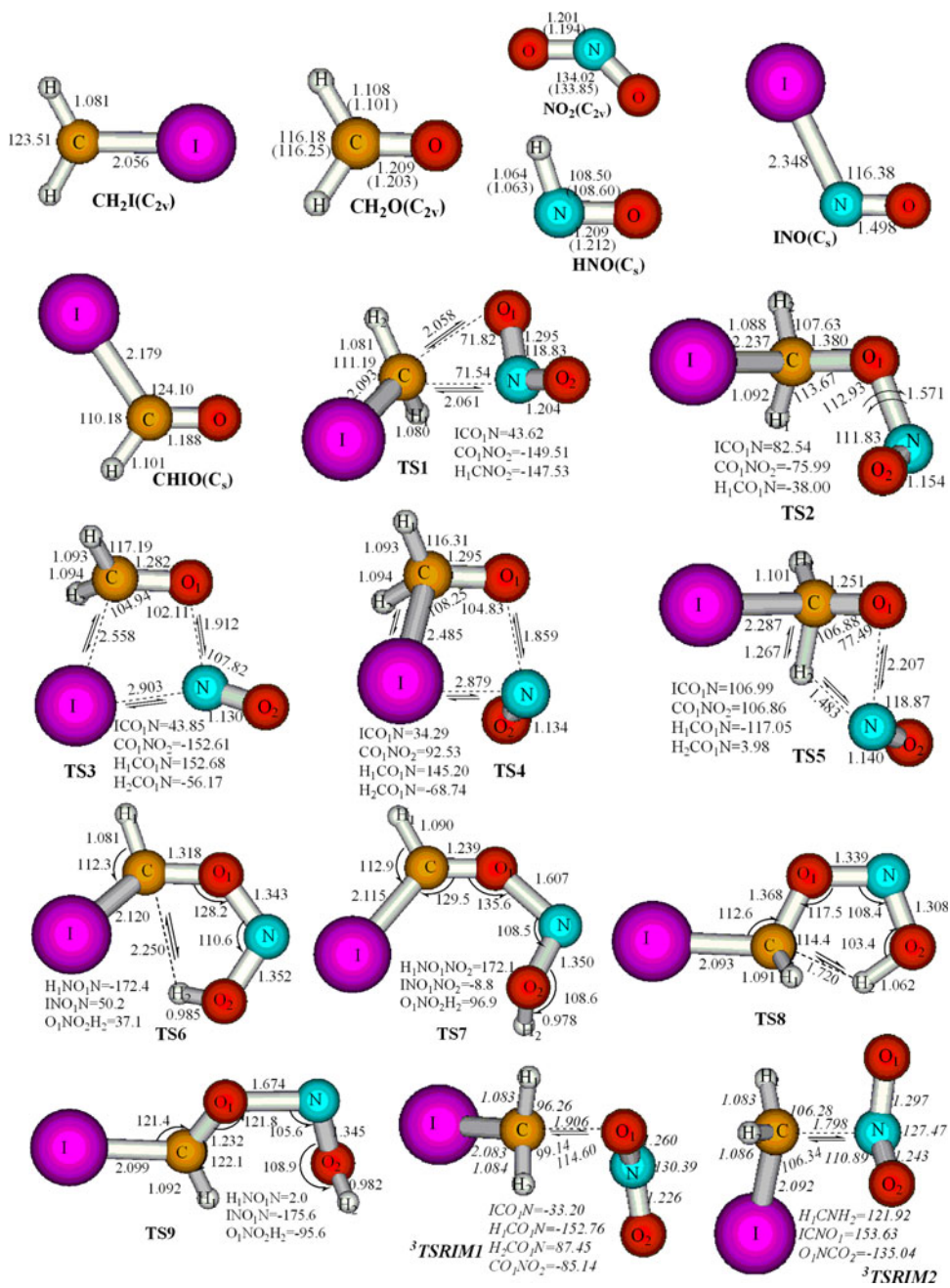
3 Results and discussion

The optimized structures of important stationary points as well as the corresponding experimental values [19, 20] for $\text{CH}_2\text{I} + \text{NO}_2$ reaction are depicted in Fig. 1, along with the vibrational mode of the imaginary frequencies of the transition states. The electronic states, harmonic vibrational frequencies of important stationary points including available experimental values [21] are listed in Table 1. Note that the calculated geometries and frequencies at the UB3LYP/I level are in good agreement with experimental results. The ZPE corrections and relative energies for most relevant species are summarized in Table 2. It is shown that relative energies at UCCSD(T)/II//UB3LYP/I and UQCISD(T)/II//UB3LYP/I levels are in good accordance. The optimized structures of intermediates and the isomers of IM2 for the title reaction are presented in Fig. 2. To clarify the reaction mechanism, the most relevant pathways of the singlet PES for $\text{CH}_2\text{I} + \text{NO}_2$ reaction at the UCCSD(T)/II level are depicted in Fig. 3. The isomerization and dissociation channels are plotted in Fig. 4. The total energy of the reactant system was obtained by addition of the energies of the doublet molecules for the title reaction. To make our discussion easier, the total energy of the reactants R for the reaction is set to be zero for reference.

3.1 Initial association

Both singlet and triplet CH_2INO_2 PESs have been obtained for the radical–radical reaction of CH_2I (C_{2v} , ${}^2\text{B}_1$) + NO_2 (C_{2v} , ${}^2\text{A}_1$). With the different atom (N or O atom) in NO_2 approaching to C atom, different intermediates are formed, namely, IM1 ($\text{H}_2\text{ICONO-}trans$), IM2 (H_2ICNO_2), and IM3 ($\text{H}_2\text{ICONO-}cis$), respectively, which are observed products in experiment [10]. The association is expected to be fast and will play a significant role in the reaction kinetics. On the singlet PES, the carbon-to-oxygen approach is more attractive to form structures IM1 and IM3 without any encounter barrier than to form the carbon-to-nitrogen approach intermediate IM2. The intermediates IM1 and IM3 are located as two energy minima lying 229.3 and 228.9 kJ/mol below the reactants R, and also lying 21.2

Fig. 1 The UB3LYP/I optimized geometries of reactants, some important products, and transition states for $\text{CH}_2\text{I} + \text{NO}_2$ reaction. The values in *italics* are for the triplet species. The values in *parentheses* are the experimental values ([19] for NO_2 , CH_2O , [20] for HNO). In the transition states, the direction of the imaginary frequency is indicated by “ \rightleftharpoons ”. Bond distances are in angstroms and angles are in degrees



and 20.9 kJ/mol lower than IM2 (-208.1 kJ/mol), respectively. Therefore, from the energy point of view, IM1 and IM3 could be initially formed and this reaction is most likely to be initiated by the carbon-to-oxygen approach on the singlet PES. Furthermore, IM1 can isomerize to IM2 via the transition state TS1, as shown in Fig. 3. On the other hand, there is a substantial barrier of 86.1 kJ/mol (${}^3\text{TSRIM1}$) for the carbon-to-oxygen attack on the triplet PES to form ${}^3\text{IM1}$ (2.2 kJ/mol) and the carbon-to-nitrogen approach can lead to the triplet isomer ${}^3\text{IM2}$ (-230.7 kJ/mol) via the transition state ${}^3\text{TSRIM2}$ with a barrier of 62.9 kJ/mol. In view of the much higher entrance

barriers, the triplet pathways may contribute less to the $\text{CH}_2\text{I} + \text{NO}_2$ reaction compared with the singlet pathways, and thus will not be further discussed. In the following discussions, we mainly discuss the formation pathways of various products proceeding via intermediate IM1.

3.2 Isomerization and dissociation pathways

The initial adduct IM1 is a stable chain-like intermediate lying 229.3 kJ/mol below the reactants. As shown in Fig. 3, the intermediate IM1 can isomerize to another chain-like intermediate IM2 undergoing the C–N bond

Table 1 The electronic states and harmonic vibrational frequencies (cm^{-1}) of reactants, some important relevant products, isomers, and transition states at the UB3LYP/I level

Species	State	UB3LYP	Expt. ^a
CH_2I	$^2\text{B}_1$	129, 611, 848, 1,357, 3,179, 3,336	355, 611, 1,331, 3,050
NO_2	$^2\text{A}_1$	749, 1,396, 1,709	750, 1,318, 1,618
CH_2O	$^1\text{A}_1$	1,194, 1,262, 1,537, 1,819, 2,914, 2,978	1,167, 1,249, 1,500, 1,746, 2,783, 2,843
INO	$^1\text{A}'$	240, 517, 1,872	216, 470, 1,809
CHIO	$^1\text{A}'$	306, 576, 863, 1,280, 1,842, 3,028	561, 1,247, 1,776, 2,930
HNO	$^1\text{A}'$	1,561, 1,677, 2,892	1,511, 1,569, 2,854
NO	$^2\Pi$	1,980	1,904
IM1	^1A	67, 167, 247, 341, 522, 554, 750, 867, 1,086, 1,255, 1,263, 1,464, 1,810, 3,114, 3,209	
IM2	$^1\text{A}'$	46, 154, 460, 505, 673, 770, 859, 921, 1,164, 1,224, 1,396, 1,445, 1,643, 3,134, 3,230	
IM3		62, 199, 328, 370, 496, 573, 809, 891, 1,007, 1,240, 1,264, 1,449, 1,753, 3,117, 3,215	
TS1		702 <i>i</i> , 72, 115, 248, 298, 519, 697, 758, 972, 1,062, 1,200, 1,368, 1,604, 3,191, 3,334	
TS2		234 <i>i</i> , 73, 196, 288, 379, 518, 732, 840, 1,041, 1,235, 1,245, 1,469, 1,859, 3,086, 3,190	
TS3		244 <i>i</i> , 126, 156, 248, 319, 381, 528, 714, 1,050, 1,204, 1,346, 1,536, 1,990, 3,059, 3,158	
TS4		182 <i>i</i> , 82, 135, 254, 314, 455, 575, 760, 1,060, 1,204, 1,311, 1,531, 1,959, 3,049, 3,146	
TS5		625 <i>i</i> , 84, 164, 239, 274, 428, 524, 681, 952, 1,171, 1,268, 1,479, 1,701, 1,974, 3,016	

^a Experimental values from Ref. [21]

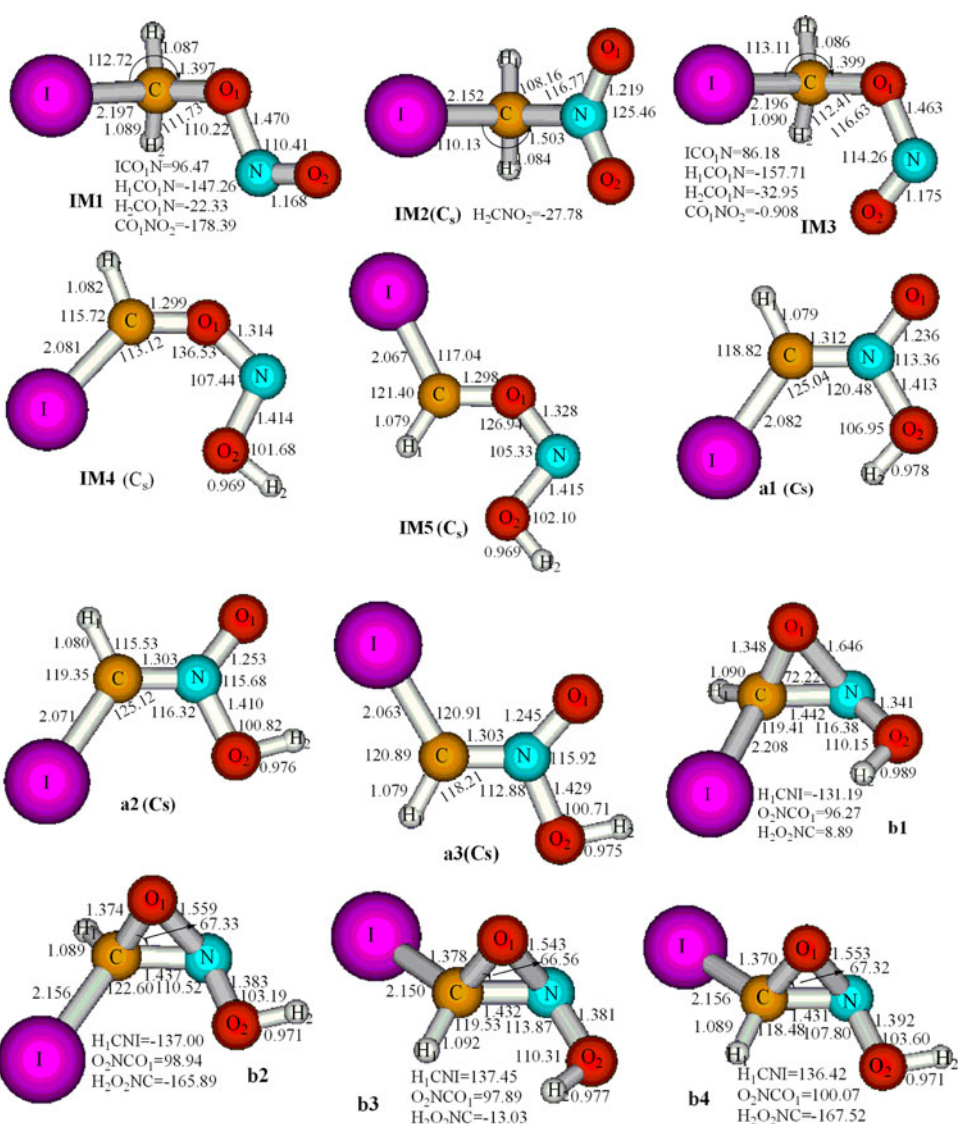
Table 2 The relative energies (kJ/mol) (including the UB3LYP/I) zero-point energy (ZPE) corrections of reactants, some important products, isomers, and transition states for the $\text{CH}_2\text{I} + \text{NO}_2$ reaction at the UCCSD(T)/II//UB3LYP/I, and UQCISD(T)/II//UB3LYP/I levels

Species	ZPE	UCCSD(T)//UB3LYP	UQCISD(T)//UB3LYP
R $\text{CH}_2\text{I} + \text{NO}_2$	0.030336	0.0	0.0
P1 $\text{CH}_2\text{O} + \text{INO}$	0.032656	-251.8	-252.5
P2 CHIO + HNO	0.031952	-221.0	-219.0
IM1	0.038086	-229.2	-229.0
IM2	0.040155	-208.1	-206.2
IM3	0.038216	-228.9	-228.8
TS1	0.035176	64.8	59.1
TS2	0.036798	-192.2	-191.5
TS3	0.036035	-173.9	-176.1
TS4	0.036085	-169.1	-170.8
TS5	0.031793	-101.7	-102.9

formation along with C–O₁ bond rupture via TS1 as shown in Fig. 1, the transition state TS1 has a loose CNO₁ three-membered ring structure, in which the length of forming C–N bond is surprisingly long as 2.061 Å, while the C–O₁ bond that will broken is 2.058 Å. The vibrational mode of frequency of TS1 corresponds to C–O and C–N bonds stretch vibration. The barrier height for this process is calculated to be 294.1 kJ/mol, which is very large to undergo. The conversion from IM1 (H₂ICONO-*trans*) to IM3 (H₂ICONO-*cis*) can be realized via O₁–N rotation transition state TS2 with small internal rotation barrier (37.0 kJ/mol above IM1). Subsequently, intermediate IM3 can dissociate to give the primary product P1 (CH₂O (C_{2v}, $^1\text{A}_1$) + INO (C_s, $^1\text{A}'$) via TS4. Furthermore, the isomers IM1 and IM3 can directly dissociate to give product P1 via C–I and N–O₁ bonds cleavage accompanied by N–I bond

formation through transition states TS3 and TS4, respectively. The dissociation barrier height for IM1 → P1 and IM3 → P1 is 55.3 and 59.8 kJ/mol, respectively. Therefore, the three pathways are feasible, with the IM1 → TS3 → P1 pathway perhaps being favored by a very small degree due to the least reaction steps and lowest overall barriers from the common intermediate IM1 to the final dissociation product P1. Both TS3 and TS4 present a loose ICO₁N four-membered ring structure, which is non-planar. The corresponding forming I–N bond lengths are 2.903 and 2.879 Å, while the breaking C–I and O₁–N distances are 2.558 and 1.912 Å (in TS3), 2.485 and 1.859 Å (in TS4). The imaginary frequency of respective 244*i* and 182*i* mainly involves the simultaneous stretch vibrations of C–I, O₁–N, and I–N bonds. Alternatively, IM1 can take a 1, 3-H shift and O₁–N bond rupture leading

Fig. 2 The UB3LYP/I optimized geometries of intermediates and the isomers of IM2 for reaction $\text{CH}_2\text{I} + \text{NO}_2$ reaction. Bond distances are in angstroms and angles are in degrees



to product P2 CHIO ($\text{C}_s, ^1\text{A}'$) + HNO ($\text{C}_s, ^1\text{A}'$) via TS5 with the barrier height 127.6 kJ/mol. The loose $\text{H}_2\text{CO}_1\text{N}$ four-membered ring, which is slightly nonplanar, is found in TS5. The migrating hydrogen is 1.267 Å away from the origin (C atom) and 1.483 Å away from the migrating terminus (N atom), and the breaking O_1-N bond is surprisingly long as 2.207 Å. In addition, the primary product P1 can further dissociate to give P3 CH_2O ($\text{C}_{2v}, ^2\text{A}_1$) + I + NO ($\text{C}_{\infty v}, ^2\Pi$) via the direct N–I single bond rupture. These processes can be simply described as:

Path1 : R → IM1, IM3 → P1($\text{CH}_2\text{O} + \text{INO}$)
→ P3($\text{CH}_2\text{O} + \text{I} + \text{NO}$)

Path2 : R → IM1 → P2(CHIO + HNO)

Furthermore, isomer IM3 can undergo a 1, 4-H shift from C to O atom via TS6 and TS8 to form the isomers IM4 and

IM5, respectively, which are *cis-trans* species for the HICONOH ($\text{C}_s, ^1\text{A}'$) structure. Note that the transition state TS6 lies 23.6 kJ/mol above the reactants R, while TS8 is 24.2 kJ/mol higher than R. Subsequently, IM4 and IM5 can dissociate to give the product P4 CHIO + HON ($\text{C}_s, ^1\text{A}'$) via the O_1-N bond rupture transition states TS7 and TS9 with a barrier of 28.2 and 37.2 kJ/mol, respectively. Starting from IM3, the channel IM3 → TS6 → IM4 → TS7 → P4 should be more favorable than the channel IM3 → TS8 → IM5 → TS9 → P4, because the rate-determining transition state TS7 lies 9 kJ/mol lower than TS9. The C_1 symmetrical TS6 and TS8 both have $\text{H}_2\text{CO}_1\text{NO}_2$ five-membered ring structure. The migrating hydrogen is 2.250 and 1.720 Å away from C atom, respectively, and 0.985 and 1.062 away from O₂ atom, respectively. The imaginary frequency is 138*i* and 568*i*, respectively, corresponding to

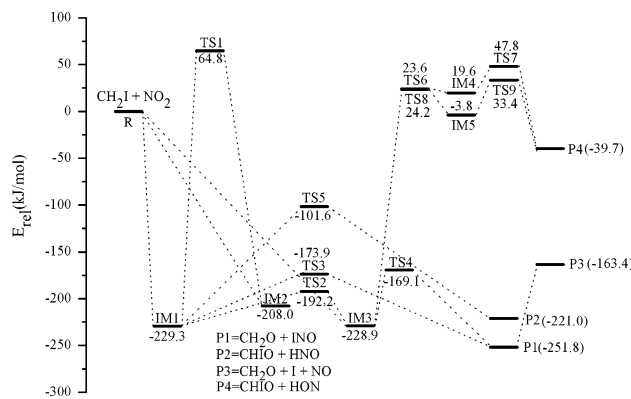


Fig. 3 Schematic singlet potential energy surface of the reaction channels for the $\text{CH}_2\text{I} + \text{NO}_2$ reaction at the UCCSD(T)/II//UB3LYP/I + ZPE level. E_{rel} are the relative energies (kJ/mol)

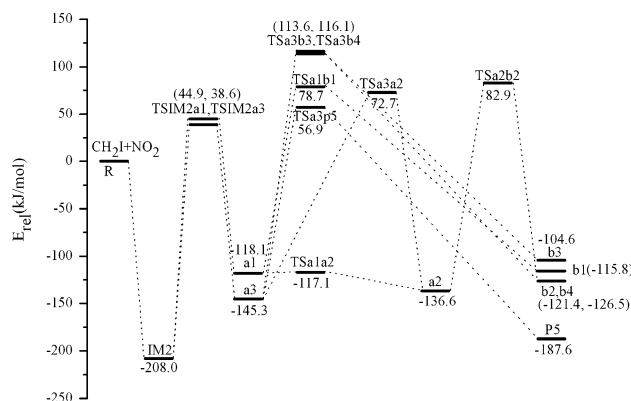


Fig. 4 The isomerization of the intermediates for the reaction of $\text{CH}_2\text{I} + \text{NO}_2$

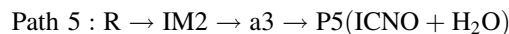
the simultaneous stretch vibrations of C-H₂ and O₂-H₂ bonds. TS7 and TS9 both are characterized by slightly elongated O₁-N bond, which indicates that species CHIO and HON are formed. Both of TS7 and TS9 have C₁ symmetry with the O₁-N bond stretch vibration for the vibrational mode of imaginary frequency of 381*i* and 274*i*, respectively. Such processes can be described as:



Because TS6, TS7, TS8, and TS9 are 23.6, 47.9, 24.2, and 33.4 kJ/mol higher than reactants R, respectively, the Paths 3 and 4 are kinetically less feasible at normal temperature and have negligible contributions to the $\text{CH}_2\text{I} + \text{NO}_2$ reaction compared with the Paths 1 and 2.

Now, we turn our attention to the other isomerization and dissociation channels of the isomer IM2, as presented in Fig. 4. First, a 1, 3-H shift from C atom to O₂ atom associated with a concert twist of IM2 can form a1 or a3. We found that the transition state TSIM2a1 lies 44.9 kJ/mol above the reactants R, while TSIM2a3 is 38.6 kJ/mol

higher than R. Therefore, formation of isomer a3 is more preferable than that of a1. a1, a2, and a3 are *cis-trans* isomers for the HICN(O)OH structure in terms of C-bound iodine or O-bound hydrogen. In addition, isomer a1 can readily convert to a2 via the N-O₂ single bond rotation transition state TSa1a2 with a small barrier height of 1.0 kJ/mol, and the conversion of a3 → a2 is a process of C=N double bond rotations via the transition state TSa3a2 with the high barrier height of 218.0 kJ/mol, while no transition state for the conversion of a1 → a3 was found. Because the a1 → a3 conversion involve a concerted process of C=N double bond and N-O₂ single bond simultaneous rotations, the high barrier may be faced for it. Subsequently, the ring-closure of a1, a2, and a3 may lead to the three-membered ring isomer b (HIC(O)NOH) including b1, b2, b3, b4. Moreover, a3 can dissociate directly to give the product P5 ICNO (C_s, ¹A') + H₂O (C_{2v}, ²A₁) via side-H₂O cleavage. Such a process can be described as:



However, the conversion transition states TSIM2a1, TSIM2a3, TSa1b1, TSa2b2, TSa3b3, TSa3b4, and TSa3P5 involved in IM2 → a1, IM2 → a3, a1 → b1, a2 → b2, a3 → b3, a3 → b4, and a3 → P5 conversion processes lie 38.6, 38.6, 78.8, 82.9, 113.6, 116.1, and 57.0 kJ/mol higher than the reactants R, respectively, as shown in Fig. 4. Clearly, the formation Paths of a (a1, a2, a3), b (b1, b2, b3, b4) and P5 are less competitive than Paths 1 and 2 at room temperature.

3.3 Reaction mechanism

As presented in the preceding sections, we have obtained four important reaction channels (Paths 1–4) for the $\text{CH}_2\text{I} + \text{NO}_2$ reaction. The CH_2I radical can barrierlessly react with NO_2 at the side-O site to form the low-lying adduct IM1 ($\text{H}_2\text{ICONO}-\text{trans}$) and IM3 ($\text{H}_2\text{ICONO}-\text{cis}$). Furthermore, isomer IM1 most favorably isomerizes to IM3 involved in Path 1. Starting from IM3, the less competitive pathways should be Path 3 and Path 4, because the rate-determining transition states TS6 (23.6 kJ/mol) and TS8 (24.2 kJ/mol) lie much higher than TS3 (-173.9 kJ/mol) and TS4 (-169.1 kJ/mol) in Path 1, TS5 (-101.7 kJ/mol) in Path 2. Subsequently, let us compare the feasibility of Path1 and Path2. Starting from IM1 and IM3, Path 1 leading to product P1 ($\text{CH}_2\text{O} + \text{INO}$) is more feasible than Path 2 starting from IM1 to form P2 ($\text{CHIO} + \text{HNO}$) because the transition states TS3 (-173.9 kJ/mol) and TS4 (-169.1 kJ/mol) in Path 1 lie 72.2 and 67.4 kJ/mol lower than TS5 (-101.7 kJ/mol) in Path 2, respectively. On the other hand, products P1 and P2 lie at 251.8 and 221.0 kJ/mol lower than the reactants R, respectively. So the

formation of P1 is more thermodynamically favorable than P2. When secondary dissociation procedure is considered, the direct N–I single bond rupture of INO in P1 to form the secondary product P3 ($\text{CH}_2\text{O} + \text{I} + \text{NO}$) may become possible after surmounting the dissociation barrier of 64.1 kJ/mol. Therefore, reflected in final product distributions, we predict that: (1) P1 may be the most feasible product with a largest yield; (2) P2 may be the second favorable products. (3) The primary product P1 ($\text{CH}_2\text{O} + \text{INO}$) can further dissociate to the secondary product P3 ($\text{CH}_2\text{O} + \text{I} + \text{NO}$).

To further testify the reaction mechanism obtained at the UCCSD(T)/II//UB3LYP/I level, we performed additional UQCISD(T)/II single-point energy calculations for the most relevant species based on the UB3LYP/I geometries. As given in Table 2, the UQCISD(T)/II and UCCSD(T)/II level are in good agreement with each other. The largest deviation between the two levels is 5.7 kJ/mol for TS1. However, such discrepancies will not affect our discussion on the reaction mechanism. It is useful to make comparison for mechanism of the $\text{CH}_2\text{I} + \text{NO}_2$ reaction between the UCCSD(T) and UQCISD(T) single-point levels. It is easily found from Table 2 that the features of PES obtained at the UQCISD(T)//UB3LYP level are in general consistent with that at the UCCSD(T)//UB3LYP level. (1) Paths 1 and 2 are both thermodynamically and kinetically feasible channels. (2) Most importantly, the high level calculations predict that Path 1 is more competitive than Path 2 because the relative energies of TS3 and TS4 in Path 1 are lower than that of TS5 in Path 2 and product P1 (−251.8 kJ/mol) is stabler than P2 (−221.0 kJ/mol).

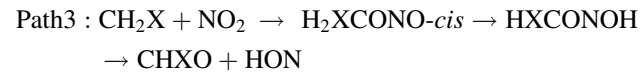
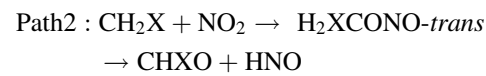
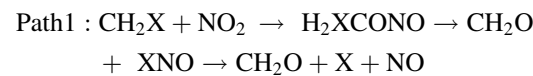
3.4 Experimental implications

Our results are in good agreement with kinetic study results by Timonen et al. [10]. For the $\text{CH}_2\text{I} + \text{NO}_2$ reaction, the observed major product is CH_2O , which can be found as one species of the most favorable product P1 ($\text{CH}_2\text{O} + \text{INO}$) in our calculations. In addition, Timonen reported that a relatively weak signal for the formation of iodonitromethane (H_2ICNO_2) or iodomethyl nitrite (H_2ICONO) product was observed, which is IM1, IM2, and IM3 in our calculation results. Formation of NO was also detected, but due to the production of other radicals than CH_2I in the photolysis or in the secondary chemistry and their possible reactions with NO_2 to produce NO, it is impossible to assign the origin of NO unambiguously to the $\text{CH}_2\text{I} + \text{NO}_2$ reaction in the experiment of Timonen et al. While, based on our present calculations, we make sure that the further dissociation of INO in primary P1 can produce species NO. Timonen et al. stated that “For the reaction $\text{CH}_2\text{I} + \text{NO}_2$ other potential products of this reaction that were searched for but not detected.”

Therefore, further kinetic investigations are still required for the unobserved products INO, CHIO, I, and HNO for $\text{CH}_2\text{I} + \text{NO}_2$ reaction to deeply understand the mechanism of the title reaction. In addition, the reaction of $\text{CH}_2\text{I} + \text{NO}_2$ is expected to contribute to the elimination of nitrogen dioxide pollutants and may be of significance in atmospheric chemistry.

3.5 Comparison between the reactions of CH_2I , and CH_2Br with NO_2

It is interesting to compare the PES feature of the $\text{CH}_2\text{I} + \text{NO}_2$ reaction with that of the analogous one $\text{CH}_2\text{Br} + \text{NO}_2$. Recently, we studied in detail the single PES of the $\text{CH}_2\text{Br} + \text{NO}_2$ reaction [11]. By comparison, it is readily found that the features of PESs on the $\text{CH}_2\text{X} + \text{NO}_2$ ($\text{X} = \text{I}$ and Br) reactions are almost in parallel. The reaction pathways leading to the feasible products (including the secondary dissociation pathways) can be summarized as:



As we can see, all these three pathways involve the same side $-\text{O}$ association process $\text{CH}_2\text{X} + \text{NO}_2 \rightarrow \text{H}_2\text{XCONO}$ ($\text{X} = \text{I}$ and Br). For the two reactions, isomers H_2XCONO ($\text{X} = \text{I}$ or Br) can undergo 1, 3- X ($\text{X} = \text{I}$ or Br) migration from C to N atom associated with $\text{N}-\text{O}_1$ weak bond cleavage leading to species $\text{CH}_2\text{O} + \text{XNO}$ ($\text{X} = \text{I}$ or Br) as the most favorable products. The fragment XNO in the most favorable product can further dissociate to form X ($\text{X} = \text{I}$ or Br) atom and NO. The primary product $\text{CHXO} + \text{HNO}$ ($\text{X} = \text{I}$ and Br) can be obtained for both reactions $\text{CH}_2\text{I} + \text{NO}_2$, and $\text{CH}_2\text{Br} + \text{NO}_2$ (via Path 2) with a comparable yield. The difference in Path 2 is that there is only one transition state (TS5) for reaction $\text{CH}_2\text{I} + \text{NO}_2$, while for $\text{CH}_2\text{Br} + \text{NO}_2$, there are two transition states leading to P2. It may due to the sterically hindered of iodine atom. For both reactions, the product $\text{CHXO} + \text{HON}$ ($\text{X} = \text{I}$ and Br) can also be obtained and it has less contribution to both reactions. Furthermore, the reactivity of the two $\text{CH}_2\text{X} + \text{NO}_2$ reactions can be discussed in the terms of the Allned–Rochow electronegativity of I (2.56) and Br (2.76) [22]. Because the I atom with smaller electronegativity strongly attracts a single electron located at the C atom, the electron density on the C atom is reduced, which leads to a increasing of the

reactivity of C atom in CH_2I attack on the O atom in NO_2 . The predicted reactivity order for $\text{CH}_2\text{I} + \text{NO}_2$ and $\text{CH}_2\text{Br} + \text{NO}_2$ is in accord with the experimental results, i.e. the measured rate constants at 298 K of $\text{CH}_2\text{X} + \text{NO}_2$ are $(2.18 \pm 0.07) \times 10^{-11}$ and $(1.76 \pm 0.03) \times 10^{-11}$ $\text{cm}^3 \text{mol}^{-1} \text{s}^{-1}$ for $\text{X} = \text{I}$ and Br , respectively. Furthermore, it is interesting to note that TS4 is the transition state of the determining process for $\text{CH}_2\text{I} + \text{NO}_2$ to produce the most feasible product P1, and in the $\text{CH}_2\text{Br} + \text{NO}_2$ reaction system, the corresponding determining process transition state is TS5 [11]. Note that the pseudopotential was employed for I atom. The barrier height (by taking the energy of corresponding reactants as reference) of the two reactions lie in the distinct difference, i.e. -169.1 and 141.9 kJ/mol using the UCCSD(T)/UB3LYP method, respectively. Thus, theoretically, the trend of reactivity is $\text{CH}_2\text{I} + \text{NO}_2 > \text{CH}_2\text{Br} + \text{NO}_2$.

4 Conclusions

The detailed singlet PES surveys including 12 isomers and 18 transition states of the $\text{CH}_2\text{I} + \text{NO}_2$ reaction systems have been characterized at the UB3LYP, and UCCSD(T) (single-point) levels. The mechanism can generally be summarized as association, isomerization, and dissociation processes.

- For the $\text{CH}_2\text{I} + \text{NO}_2$ reaction, with the different atom (N or O atom) in NO_2 approaching to C atom, different initial intermediates are formed, namely, IM1 ($\text{H}_2\text{ICONO-}trans$), IM2 (H_2ICNO_2), and IM3 ($\text{H}_2\text{ICONO-}cis$), respectively.
- Starting from IM1, two primary products P1 ($\text{CH}_2\text{O} + \text{INO}$) and P2 ($\text{CHIO} + \text{HNO}$), and one secondary product P3 ($\text{CH}_2\text{O} + \text{I} + \text{NO}$) should be observed. P1 may be the most feasible product with a largest yield, and P2 may be the second favorable products. Our results agree well with the experimental observation for $\text{CH}_2\text{I} + \text{NO}_2$ reaction.
- The PES features of the $\text{CH}_2\text{I} + \text{NO}_2$ and $\text{CH}_2\text{Br} + \text{NO}_2$ reactions are similar. The triplet pathways have much less competitive abilities for both reactions and can thus be neglected. The present theoretical studies may provide useful information on

the reaction mechanism and assist in further laboratory identification of the products for the title reaction. From electronegativity and barrier height analysis, we predicted that reaction $\text{CH}_2\text{I} + \text{NO}_2$ is faster than $\text{CH}_2\text{Br} + \text{NO}_2$, which is in accord with the experimental results.

Acknowledgments This work is supported by the Training Fund of NENU'S Scientific Innovation Project (NENU-STC07016). We are greatly thankful for the referees' helpful comments.

References

- NIST Chemical Kinetics Database, Standard Reference Database 17, Version 7.0 (Web Version), Release 1.2, National Institute of Standards and Technology, Gaithersburg, MD
- Alicke B, Hebestreit K, Stutz J, Platt U (1999) Nature 397:572
- Lovelock JE, Maggs RJ, Wade RJ (1973) Nature 241:194
- Jordan A, Harnisch J, Borchers R, Guern Fle, Shinohara H (2000) Environ Sci Technol 34:1122
- Baren RE, Erickson M, Hershberger JF (2002) Int J Chem Kinet 34:12
- Rim KT, Hershberger JF (1998) J Phys Chem A 102:4592
- Lanier WS, Mulholland JA, Beard JT (1988) Symp Int Combust Proc 21:1171
- Chen SL, McCarthy JM, Clark WD, Heap MP, Seeker WR, Pershing DW (1988) Symp Int Combust Proc 21:1159
- Faravelli T, Frassoldati A, Ranzi E (2003) Combust Flame 132:188
- Eskola AJ, Pastuszka DW, Ratajczak E, Timonen RS (2006) J Phys Chem A 110:12177
- Jia XJ, Pan XM, Sun JY, Tang YZ, Sun H, Pan YR, Wang RS (2009) Theor Chem Acc 122:207
- Frisch MJ, Trucks GW, Schlegel HB et al (2004) Gaussian 03, revision C.02. Gaussian, Inc., Wallingford
- Becke AD (1993) J Chem Phys 98:5648
- Lee C, Yang W, Parr RG (1988) Phys Rev B 37:785
- Dunning TH Jr (1989) J Chem Phys 90:1007
- Dunning TH Jr, Peterson KA, Wilson AK (2001) J Chem Phys 114:9244
- Gonzalez C, Schlegel HB (1989) J Chem Phys 90:2154
- Gonzalez C, Schlegel HB (1990) J Phys Chem 94:5523
- Kuchitsu K (1998) Structure of free polyatomic molecules basic data. Springer, Berlin
- Lide DR (1999) CRC handbook of chemistry and physics, 80th edn. CRC Press, Boca Raton
- In NIST Chemistry WebBook. NIST standard reference database number 69 (2005) release (vibrational frequency data compiled by ME Jacox)
- “Cotton FA, Wilkinson G, Murillo CA, Bochmann M (1972) Adv Inorganic Chem. 3rd U.S. edn., pp 384–401